



Geothermal gradient distributions in parts of the northern Cretaceous Benue Trough of Nigeria: a look at high-resolution aeromagnetic data

Oparaku O. I¹, Onuba, L.N², Umego M.N³, Onyebueke³ O.E., Asoegwu, I.K³.

1 Federal Polytechnic Nekede, Department of Physics/Electronics, Owerri, Nigeria

2 Chukwuemeka Odumegwu Ojukwu University, Department of Geology, Uli, Nigeria

3 Chukwuemeka Odumegwu Ojukwu University, Department of Industrial Physics, Uli, Nigeria

Corresponding author's email: oparakukatchy79@gmail.com

Abstract: Heat flow distribution and geothermal resources detection are accessed by the combination of spectral analysis of aeromagnetic data and application of one-dimensional Fourier heat law. Spectral analysis techniques were employed to evaluate aeromagnetic anomalies of the northern Benue Trough, covering about 48,400 square kilometres of the area. On the average, depth to the magnetic basement varies from 300 m to 1900 m for shallow anomaly sources while for deeper sources vary from 2700 to 8000 m. The results reveal that sediments are thinnest in the northeast parts where volcanic rocks predominate but high at the north-western part of the study area. The Curie point depths estimated vary from about 5 km around Biu areas to less than 15 km in the Dukku area. The results perhaps show the study area could likely be composed of mainly thin magnetised crust. Three zones of geothermal gradients identified are: 38 - 60°C/km for zone of low geothermal gradient, 60 - 100°C/km for zone of intermediate geothermal gradient and over 100°C/km for zone of high geothermal gradient. The results reveal that zones of the intermediate geothermal gradient lie within the oil generating window and could have moderate hydrocarbon potentials. While the zone of high geothermal gradient lies within the non-volcanic portion and could serve as renewable-energy potentials for the region.

Keywords: aeromagnetic data, spectral analysis, geothermal gradient and volcanic rocks.

Introduction

The energy-shift from fossil-fuel energy to non-hydrocarbon energy resources has led to massive explorations on the earth's crust. Geothermal energy is renewable and environmental-friendly energy from radioactive crustal rocks or intrusive from earth's interior. Nigeria is currently experiencing a low production and distribution of fossil power. Hence, the harness of geothermal energy will reduce the absolute dependency on fossil fuels and give direct industrial and domestic applications like heating and cooking.

Geothermal resource potentials sometimes can be identified by the presence of hot springs, hot dry rocks, geysers and increased geothermal gradient of the rocks. The normal thermal value for continental regions is an average heat flow of about 60mWm^{-2} . The heat flow values between $80\text{-}100\text{mWm}^{-2}$ are good geothermal source, while values greater than 100mWm^{-2} indicate anomalous conditions (Franco and Franco, 2017).

The geothermal gradient is a fundamental tool in exploration for geothermal resources. Resources are usually explored for in areas with high anomalous geothermal gradients at regions around plate boundaries or with active volcanoes (Tselentis et al., 1991). Geothermal gradients can be estimated either from well log data (Bottom-hole temperature data) or Curie point depths (CPDs) of aeromagnetic data. The fast Fourier Spectral analysis provides depths to Centroid and top of the magnetic sources. These depths form the necessary parameters for estimation of geothermal gradient and heat flux distribution. The aeromagnetic data processing enhances possible geologic features and further generates the depth estimates from radially power spectral analysis whereas Bouguer gravity data analysis informs possible heatflow sources that create the geothermal fields; Therefore, combination of magnetic and gravity methods paves a way for detail study for both geothermal gradients fields and heatflow origins.

Benue trough Nigeria houses echelons of hot springs this makes the trough a targeted location for researches. The major factor that influenced the choice of the location for the research was the geographical siting of Akiri and Wikki warm Springs of northern Benue Trough suspected geothermal fields as suggested by many authors (Odidi & Nasir 2020).

Location of the study area

The study area covers the Northern Benue Trough bounded by latitude $9^{\circ}30' - 11^{\circ}30'$ and longitude $10^{\circ}30' - 12^{\circ}30'$ (figure 1.0) and sixteen High Resolution aeromagnetic map sheets : Dukku (130) , Bajoga (131), Gulani (132), Biu (133), Ako (151), Gombe(152), Wuyo(153), Shani(154), Futuk(172), Kaltungo(173), Guyuk(174), Shellen(175), Muti(193), Lau (194), Dong (195), Numan (196) with total area of 48,400 square kilometres .

Table 1: Data sheet layout

SHEET 130 DUKKU	SHEET 131 BAJOGA	SHEET 132 GULANI	SHEET 133 BIU
SHEET 151 AKO	SHEET 152 GOMBE	SHEET 153 WUYO	SHEET 154 SHANI
SHEET 172 FUTUK	SHEET 173 KALTUNGO	SHEET 174 GUYOK	SHEET 175 SHELLEN
SHEET 193 MUTI	SHEET 194 LAU	SHEET 195 DONG	SHEET 196 NUMAN

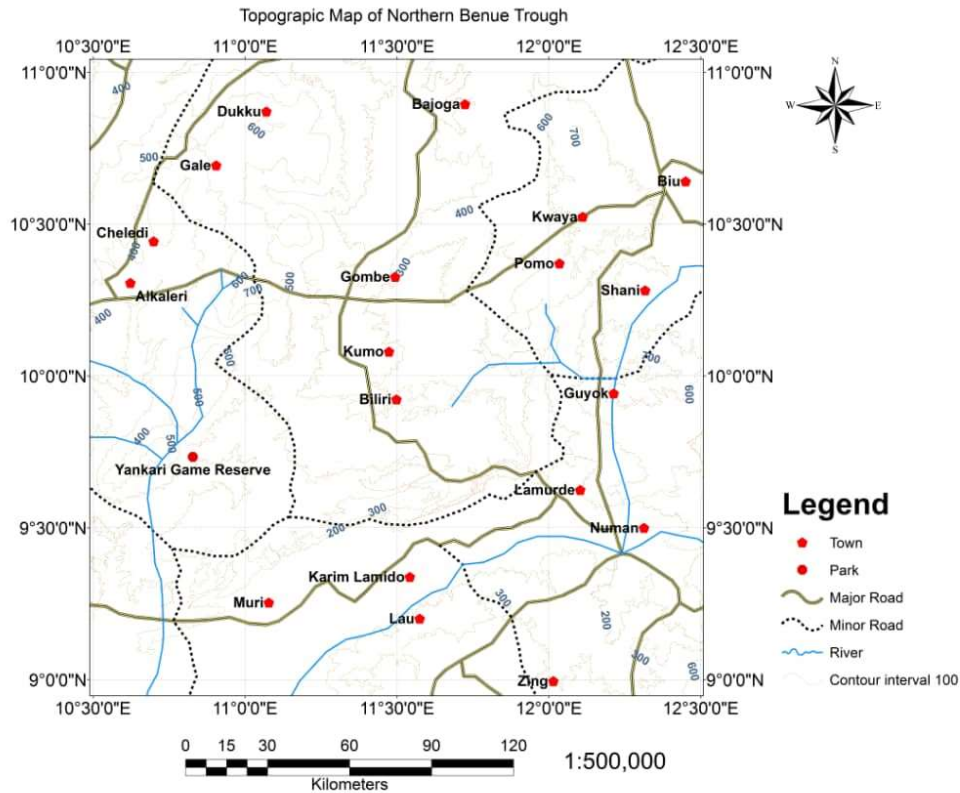


Figure 1: The Topographic Map of the study area.

The physiological features recognized in the area Gongola valley, Kerri-Kerri plateau and Biu plateau.

GEOLOGY OF THE RESEARCH AREA

The geology of the study area falls into the Benue trough of Nigeria. The Northern Benue Trough is part of the Benue Trough of Nigeria, comprised of three basins: the east–west trending Yola Basin (Yola Arm), the North– south trending Gongola Basin (Gongola Arm) and the northeast– southwest trending Lau Basin (Main Arm) covering parts of Adamawa, Gombe, Borno, Bauchi, Yobe and Taraba States of Northeastern Nigeria

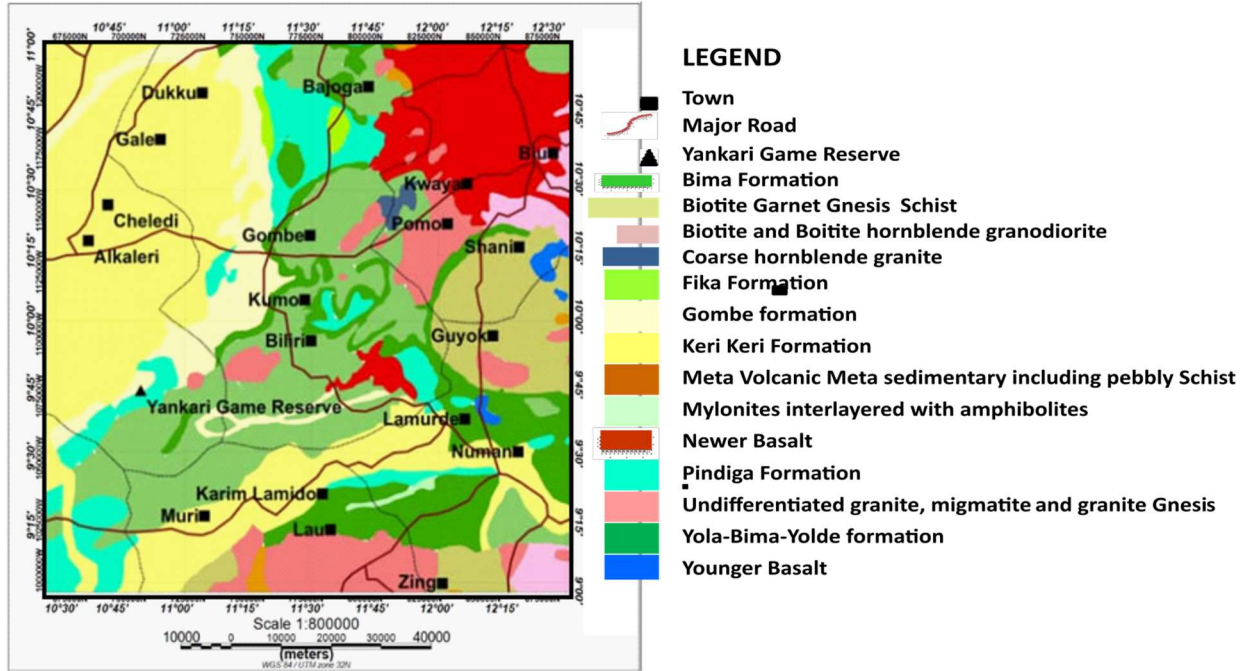


Figure 3: The geology map of the study area

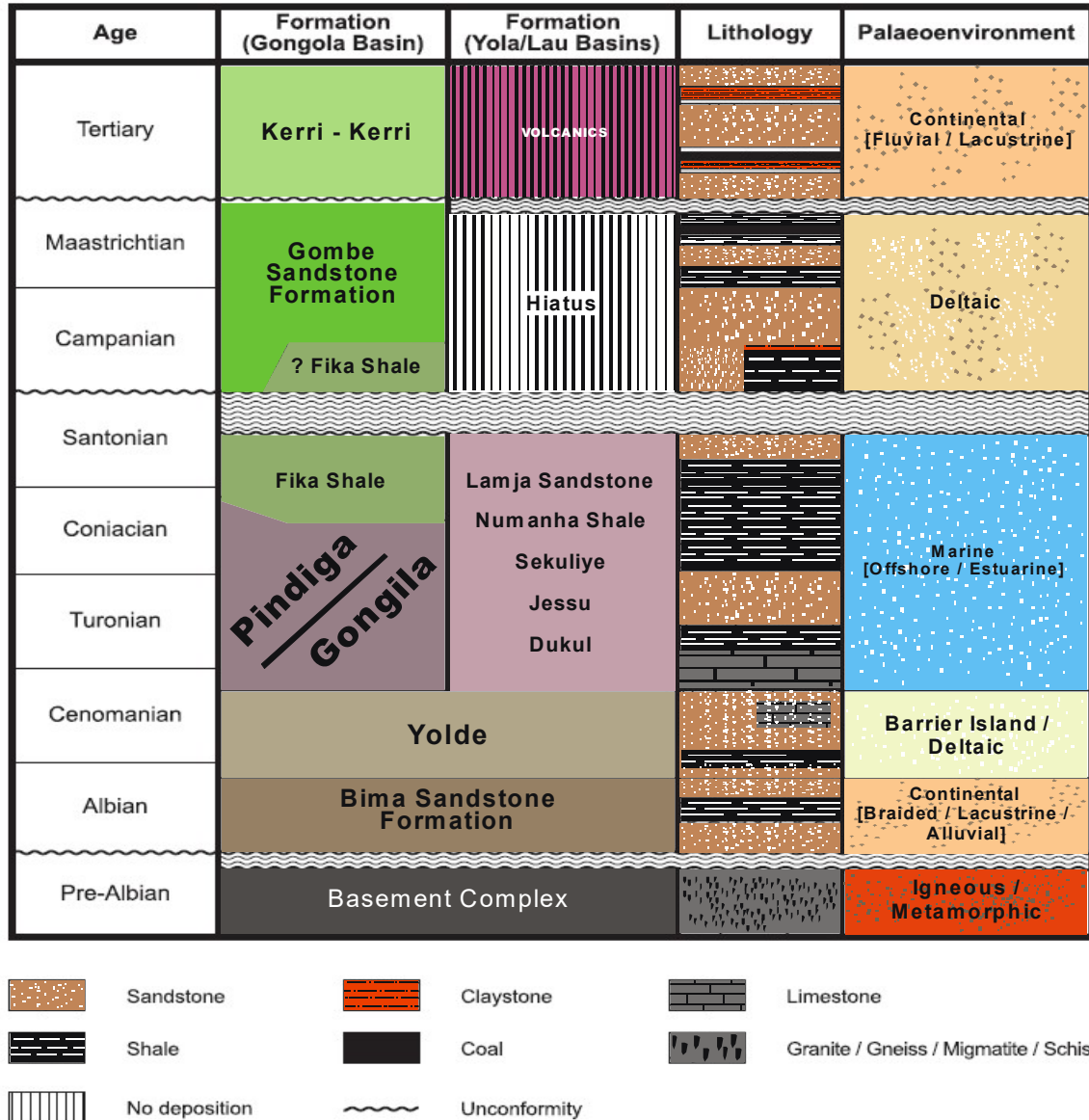


Figure 4: Stratigraphy sequence of Northern Benue Trough (Adapted from Amadu, 2015)

Materials and Method

Materials

The aeromagnetic and gravity data sets were acquired by the Nigerian Geological survey Agency between 2006 and 2010. The Sixteen (16) high resolution aeromagnetic maps used for the study were acquired in grid format. This enhanced data set has improved data quality, minimal systematic errors that would have been introduced by manual digitization of the maps. Regional magnetic value of 33,000nT was subtracted from the total field for ease of processing. The aeromagnetic grid file is then contoured using the bi-directional extension of the oasis Montaj software at a scale of 1:770,000.

Method:

Many authors have successfully used spectral analysis to estimate depths-to-top of the magnetic causative body and base of the Curie point (Akinyemi, 2019). Assuming that the magnetization of a set of two-dimensional bodies uncorrelated and randomly sampled, the radial average power density spectra of the total field anomaly can be expressed as (Blakely, 1995)

$$P(k_x k_y) = 4\pi^2 C^2 [\theta_m]^2 [\theta_f]^2 e^{-(1-e^{-1|k|(z_b-z_t)})^2} \dots \dots \dots (1)$$

Here, k_x and k_y are the wave numbers in the x- and y-directions; C is a constant of proportionality; θ_m is the power spectrum of the magnetization; θ_m and θ_f are the directional factors related to the magnetization and geomagnetic field respectively; and Z_t and Z_0 are the top and bottom depths of the magnetic sources. After annual averaging, Eq. (1) can be written as:

After annual averaging, Equation (1) can be written as:

$$P|k| = A_1 e^{-2|k|Z_t (1-e^{-|k|(Z_b-Z_t)})^2} \dots \dots \dots (2)$$

Where A_1 is a constant, k is the wave number and $P|k|$ power spectral density Equation (2) can be simplified to compute the centroid depth Z_0 of the magnetic source from the low wave number part of the power spectrum as follows:

The centroid depth is calculated from the low wavenumber part of the scaled power spectrum as:

$$\ln \left(\frac{P(K)^{\frac{1}{2}}}{K} \right) = A - |k| Z_0 \dots \dots \dots (3)$$

Where \ln is the natural logarithm, $P(k)$ is the radially average power spectrum, k is the wave number ($2\pi/km$). A is a constant depending on the properties of magnetization and its orientation and Z_0 is the centroid depth of the magnetic sources (Eko et al .2021). For the high wavenumber part, the lower spectrum can be related to the top of magnetic sources by a similar equation:

$$\ln \left(\frac{P(K)^{\frac{1}{2}}}{K} \right) = B - |k| Z_t \dots \dots \dots (4)$$

Where B is a constant: Z_t is the depth to the top of the magnetic sources.

The depth of the bottom of magnetization Z_b (Curie Point Depth) is:

$$Z_b = 2Z_0 - Z_t \dots\dots\dots (5)$$

Summarily, the depth to the base of the magnetic source (i.e. the Curie point depth) is calculated in four steps (Qudsi, 2019; Kasidi & Nur, 2021) as follows:

Step 1: Calculate the radially averaged power spectrum of the magnetic data in each window;

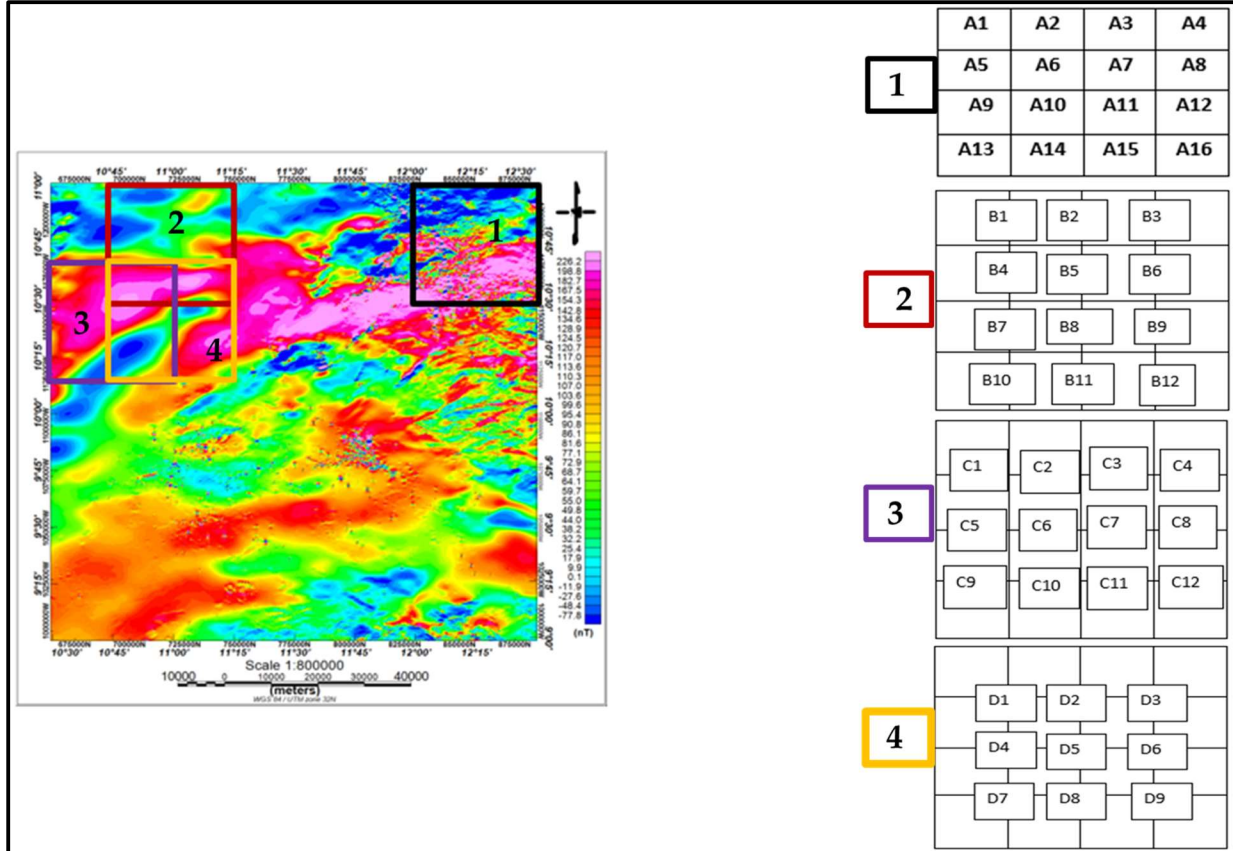


Figure 5: Spectral cell with three overlapping windows using four spectral designs (Window size used was 55 by 55 km).

Step 2: Estimate the depth to the top of the magnetic source (Z_t) using the high wave number portion of the magnetic anomaly power spectra;

Step 3: Estimate the depth to the centroid of the magnetic source (Z_0) using a lower wave number portion of the magnetic anomaly power spectra;

Step 4: Calculate the depth to the base of the magnetic source (Z_b) using $Z_b = 2Z_0 - Z_t$. The value of Z_b is the Curie point

The heat flow of the study area which has an assumption that the direction of the temperature variation is vertical and the geothermal gradient $\frac{\partial T}{\partial Z}$ is constant;

Then the Fourier's heat flow law takes the form:

$$q = -k \frac{\partial T}{\partial Z} \dots \dots \dots (6)$$

Where, q is heat flow and k is thermal conductivity

The Curie temperature $\theta^{\circ}C$ can also be defined as:

$$\theta^{\circ}C = \frac{\partial T}{\partial Z} \dots \dots \dots (7)$$

Where, ∂Z is the curie-point depth (as obtained from the spectral magnetic analysis).
Therefore the Geothermal gradient in the relation to the heat flow q.(Tanaka et al 1999):

$$q = k \frac{\theta^{\circ}c}{Z_b} \dots \dots \dots (8)$$

Curie point temperature of $580^{\circ}C$ and thermal conductivity of $2.5Wm^{-1}C^{-1}$ (Uche, 2020; Akinnubi & Adetona, 2018) which is the average thermal conductivity for igneous rocks is used in the study as standard (Abdulwahab et al, 2019).

RESULT:

Results from aeromagnetic data are best presented as processed maps for possible anomalous observation in trend and pattern of the analytical signals. These processed maps include total magnetic field intensity maps, first order derivatives, analytic signals and CET maps.

Firstly, for ease of interpretation, 33000nT was removed from the aeromagnetic data. The Total Magnetic field (TMI) map shows the magnetic intensity distribution within the Trough. The total magnetic field intensity (TMI) map exhibits a very complex array of magnetic anomalies of both short and long wavelengths. These wavelengths are represented as magnetic lows and highs from anomalous bodies. The TMI map of the study area is marked with many discontinuities and geological units. The TMI map reveals high, intermittent and magnetic zones within the research area. Theses variations in the values of the total magnetic field were as a result of lateral disposition of rocks with distinctive lithologies. The high magnetic region were predominately Ferro-magnetic rocks while low magnetic regions were of paramagnetic rock deposition. The intermediate magnetic regions represented the weathered ferromagnetic rock. The two observed lava channels of high frequency on the TMI map must have provided conduit for the flow of magnetic fluid from volcanic complex at the East to Western territories of the research area.

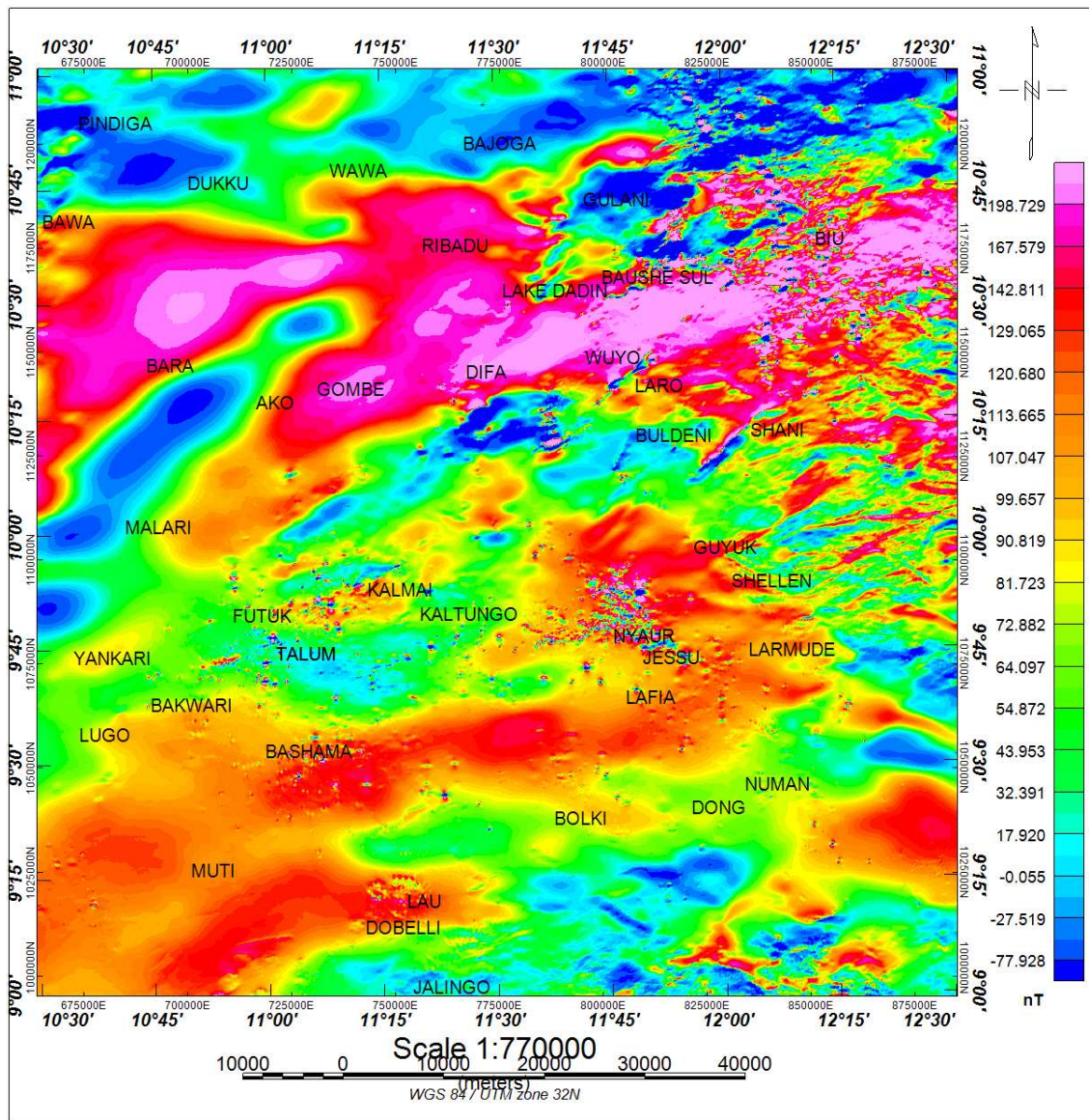


Figure 6: Total Magnetic Field Intensity (TMI) of the Northern Benue Trough

To delineate the lithological units from the aeromagnetic data, the First vertical derivative was utilized. Isolated high and low contours values signify igneous and sedimentary areas respectively. However, the existence of high magnetic zone alongside lower magnetic values depicts faults on volcanic units (Salawe. et al 2021; Zhanxiang et al 2008). Figure 2 shows about five (5) volcanic regions within the research area with fault aligning in the NE-SW trend.

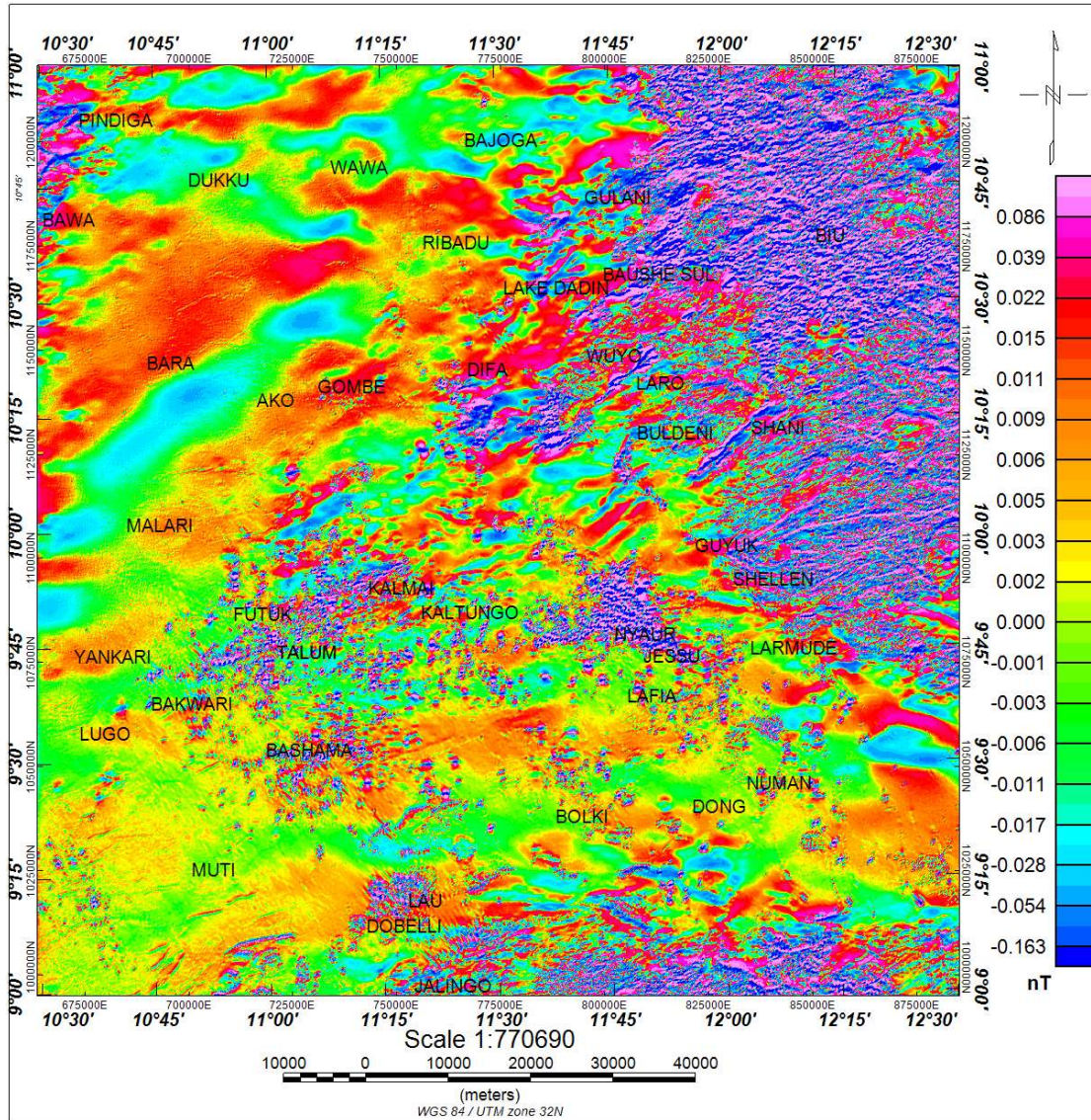


Figure 6: First vertical order derivatives

The degree of randomness is linked to thermal activities. Entropy is the ratio of energy to temperature. The CET extension of the Oasis Montaj software presents the aeromagnetic data as active or inactive regions with respect to energy related event occurrence within the research area as seen in Figure (7)

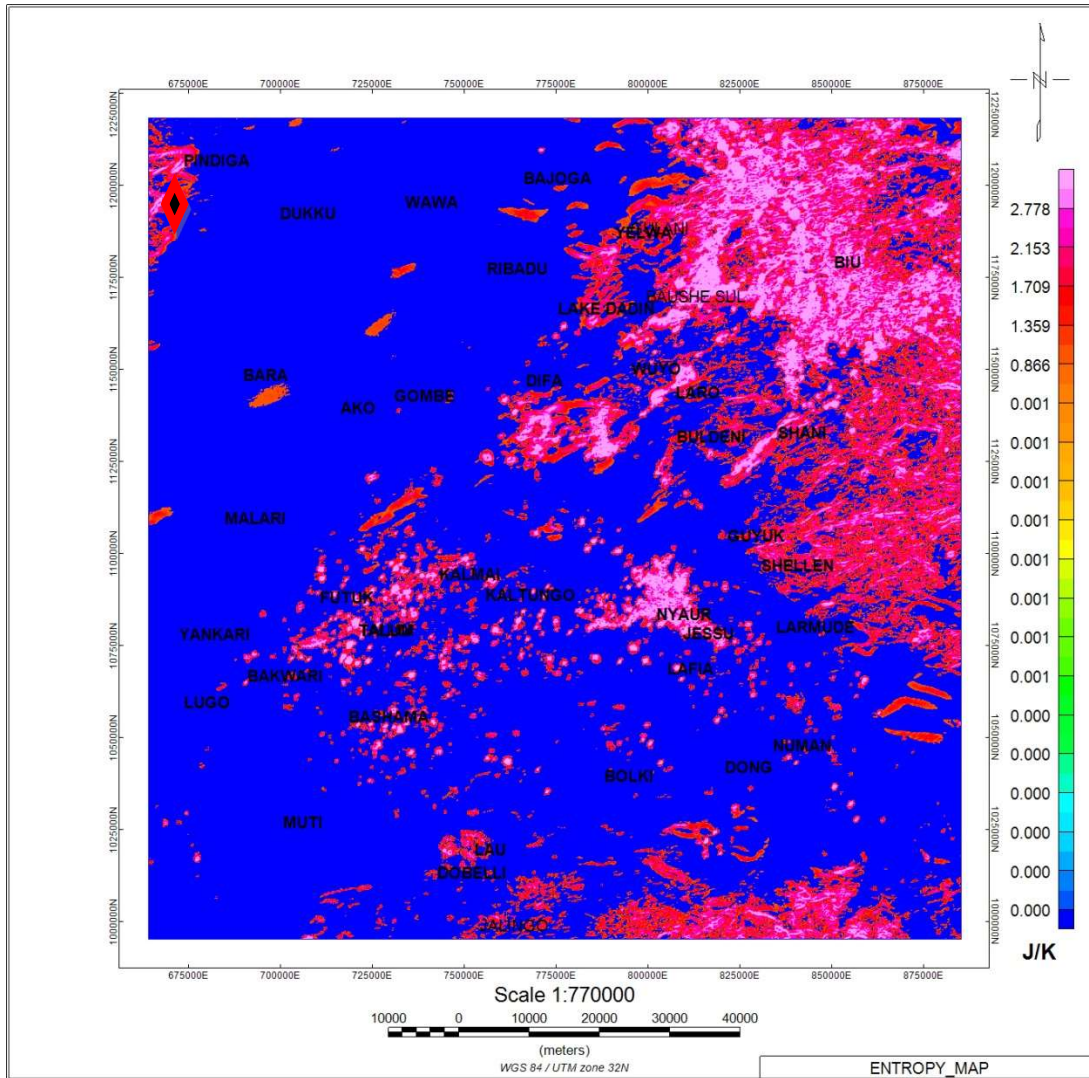


Figure 7: Entropy map derived from CET-extension of the Oasis Montaj

However, the spectral depth estimation is carried out using three (3) overlapping windows and four step techniques as shown in figure (8).

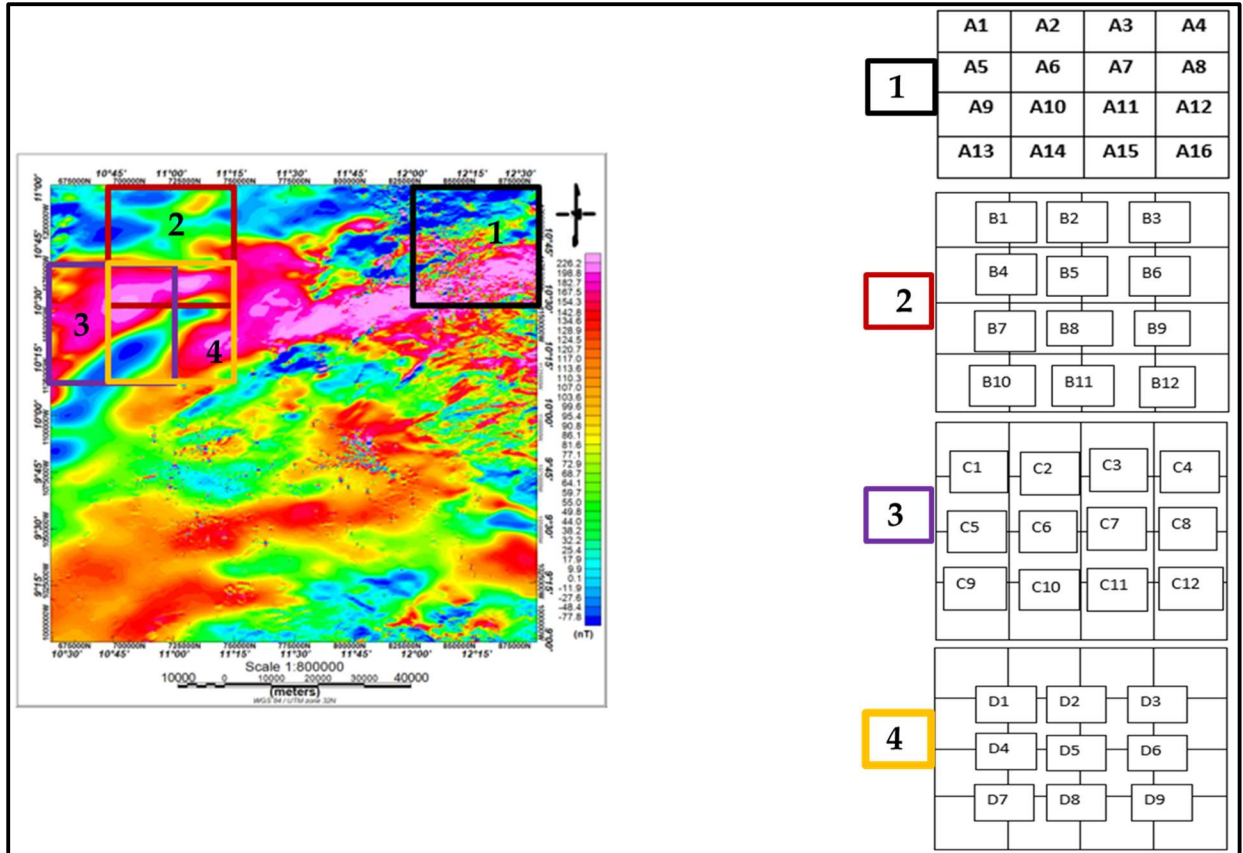


Figure 8: Spectral cell with three overlapping windows using four spectral designs (Window size used was 55 by 55 km).

The spectral depths from the forty-nine blocks were used to compute the basal/ Curie point depths hence estimate the geothermal gradient and heat flow values as tabulated in Table (2) .

Table 2: Estimated Spectral depths, Curie Point Depths, geothermal and heat flow values of study area.

S/N	Latitude	Longitude	Spectral blocks	Deeper depth (Km)	Shallower depth(km)	Curie-point depth (km)	Geothermal gradient (°C/km)	Heat flow (mWm/°C)
1	10:30-11:00	10:30-11:00	A1	5.4	1.0	9.8	59.18367	147.9592
2	10:30-11:00	11:00-11:30	A2	5	0.8	9.2	63.04348	157.6087
3	10:30-11:00	11:30-12:00	A3	4	0.5	7.5	77.33333	193.3333
4	10:30-11:00	12:00-12:30	A4	3.5	0.3	6.7	86.56716	216.4179
5	10:00-10:30	10:30-11:00	A5	8.0	1.1	14.9	38.92617	97.31544
6	10:00-10:30	11:00-11:30	A6	5.4	0.7	10.1	57.42574	143.5644
7	10:00-10:30	11:30-12:00	A7	6.0	0.6	11.4	50.87719	127.193
8	10:00-10:30	12:00-12:30	A8	2.8	0.3	5.3	109.434	273.5849
9	9:30-10:00	10:30-11:00	A9	5.5	0.8	10.2	56.86275	142.1569
10	9:30-10:00	11:00-11:30	A10	5.0	0.5	9.5	61.05263	152.6316
11	9:30-10:00	11:30-12:00	A11	4.5	0.4	8.6	67.44186	168.6047
12	9:30-10:00	12:00-12:30	A12	3.1	0.3	5.9	98.30508	245.7627
13	9:00-9:30	10:30-11:00	A13	5.3	0.6	10	58	145
14	9:00-9:30	11:00-11:30	A14	6.4	0.4	12.4	46.77419	116.9355
15	9:00-9:30	11:30-12:00	A15	5.0	0.5	9.5	61.05263	152.6316
16	9:00-9:30	12:00-12:30	A16	4.7	0.4	9.0	64.44444	161.1111
17	10:30-11:00	10:45-11:15	B1	5.0	0.8	9.2	63.04348	157.6087
18	10:30-11:00	11:15-11:45	B2	4.3	0.7	7.9	73.41772	183.5443
19	10:30-11:00	11:45-12:15	B3	3.5	0.5	6.5	89.23077	223.0769
20	10:00-10:30	10:45-11:15	B4	7.0	0.6	13.4	43.28358	108.209
21	10:00-10:30	11:15-11:45	B5	6.0	0.7	11.3	51.32743	128.3186
22	10:00-10:30	11:45-12:15	B6	3.0	0.6	5.4	107.4074	268.5185
23	9:30-10:00	10:45-11:15	B7	5.8	0.4	11.2	51.78571	129.4643
24	9:30-10:00	11:15-11:45	B8	5.0	0.5	9.5	61.05263	152.6316
25	9:30-10:00	11:45-12:15	B9	6.0	1.0	11.0	52.72727	131.8182
26	9:00-9:30	10:45-11:15	B10	6.5	0.8	12.2	47.54098	118.8525
27	9:00-9:30	11:15-11:45	B11	4.7	0.5	8.9	65.16854	162.9213
28	9:00-9:30	11:45-12:15	B12	3.2	0.4	6.0	96.66667	241.6667
29	10:15-10:45	10:30-11:00	C1	8.0	1.0	15.0	38.66667	96.66667
30	10:15-10:45	11:00-11:30	C2	4.9	0.8	9.0	64.44444	161.1111
31	10:15-10:45	11:30-12:00	C3	5.0	0.7	9.3	62.36559	155.914
32	10:15-10:45	12:00-12:30	C4	4.7	0.5	8.9	65.16854	162.9213
33	10:15-9:45	10:30-11:00	C5	6.0	0.8	11.2	51.78571	129.4643
34	10:15-9:45	11:00-11:30	C6	3.5	0.5	6.5	89.23077	223.0769
35	10:15-9:45	11:30-12:00	C7	3.7	0.4	7.0	82.85714	207.1429
36	10:15-9:45	12:00-12:30	C8	2.7	0.5	4.9	118.3673	295.9184
37	9:45-9:15	10:30-11:00	C9	5.4	1.0	9.8	59.18367	147.9592
38	9:45-9:15	11:00-11:30	C10	6.8	0.8	12.8	45.3125	113.2813

39	9:45-9:15	11:30-12:00	C11	5.7	0.6	10.8	53.7037	134.2593
40	9:45-9:15	12:00-12:30	C12	4.7	1.0	8.4	69.04762	172.619
41	10:45-10:15	10:45-11:15	D1	7.5	0.7	14.3	40.55944	101.3986
42	10:45-10:15	11:15-11:45	D2	6.0	1.0	11.0	52.72727	131.8182
43	10:45-10:15	11:45-12:15	D3	4.7	1.2	8.2	70.73171	176.8293
44	10:15-9:45	10:45-11:15	D4	4.6	1.0	8.2	70.73171	176.8293
45	10:15-9:45	11:15-11:45	D5	3.5	1.1	5.9	98.30508	245.7627
46	10:15-9:45	11:45-12:15	D6	4.3	1.3	7.3	79.45205	198.6301
47	9:45-9:15	10:45-11:15	D7	6.6	0.5	12.7	45.66929	114.1732
48	9:45-9:15	11:15-11:45	D8	4.6	0.7	8.5	68.23529	170.5882
49	9:45-9:15	11:45-12:15	D9	4.9	1.9	7.9	73.41772	183.5443

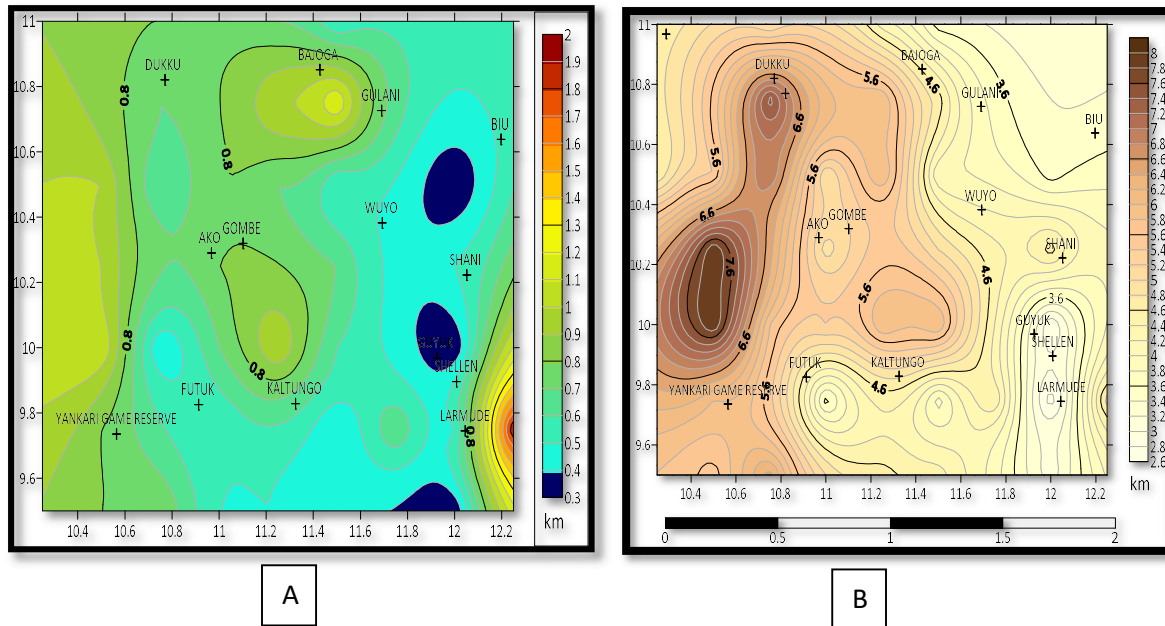


Figure 9: Depth to shallower (A) and deeper magnetic (B) sources of the research area

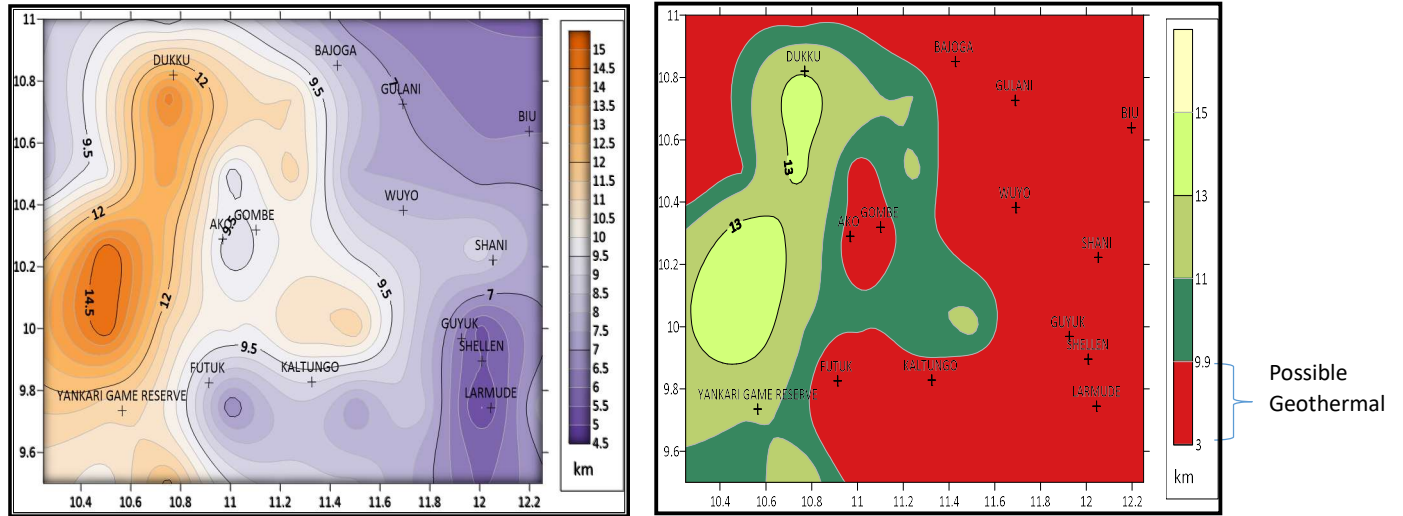


Figure 10: Curie Point Depth (CPD) within the study area

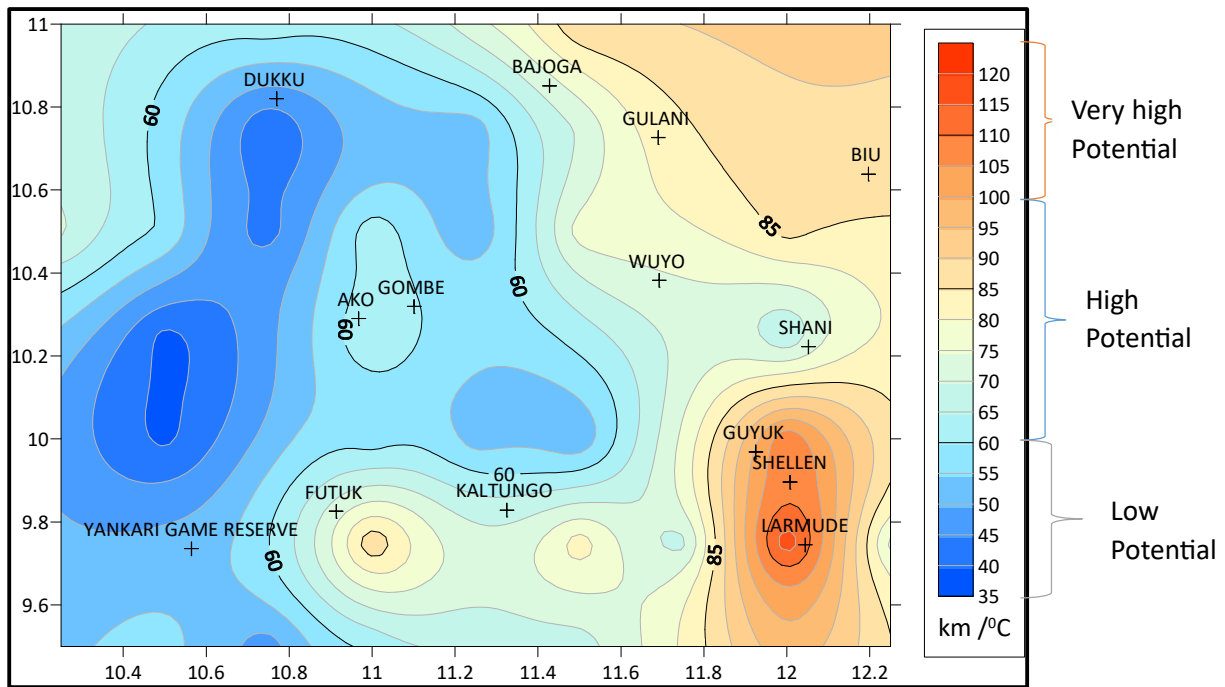


Figure 11: Geothermal gradient variation across the study area

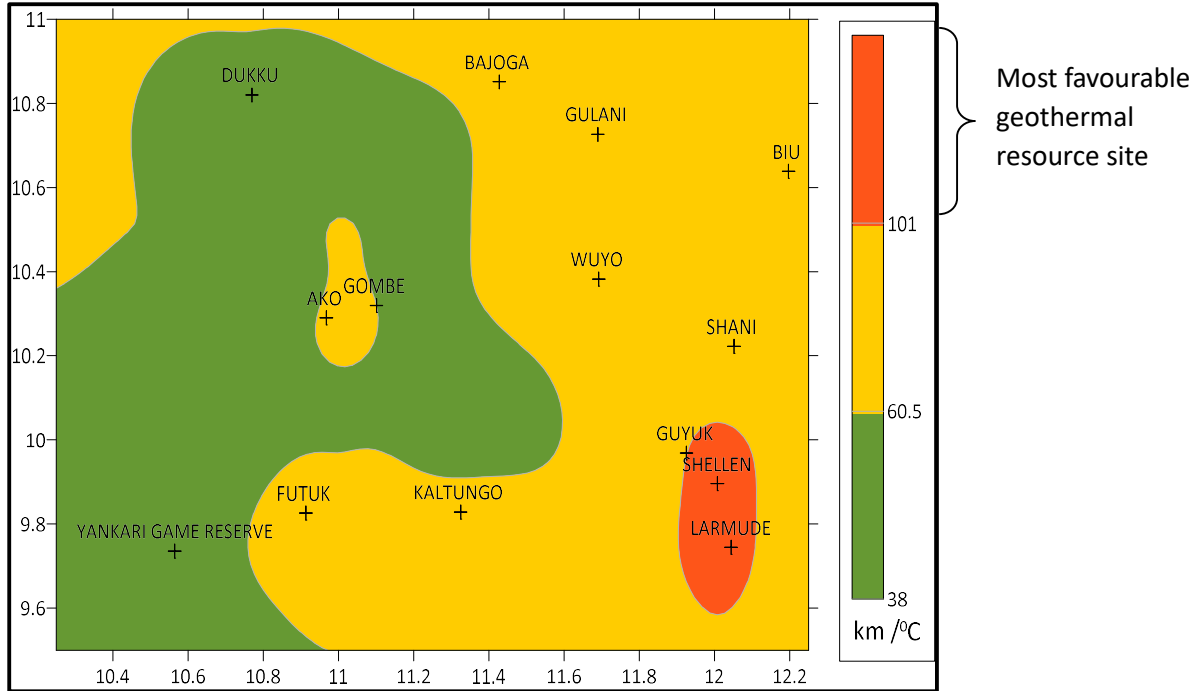


Figure 12: Proposed Geothermal zones with the study area

Heat flow variation is transient energy and has a direct proportionality with geothermal gradient. A comparative stack analysis of the dataset attests to this relationship in Figure 13.

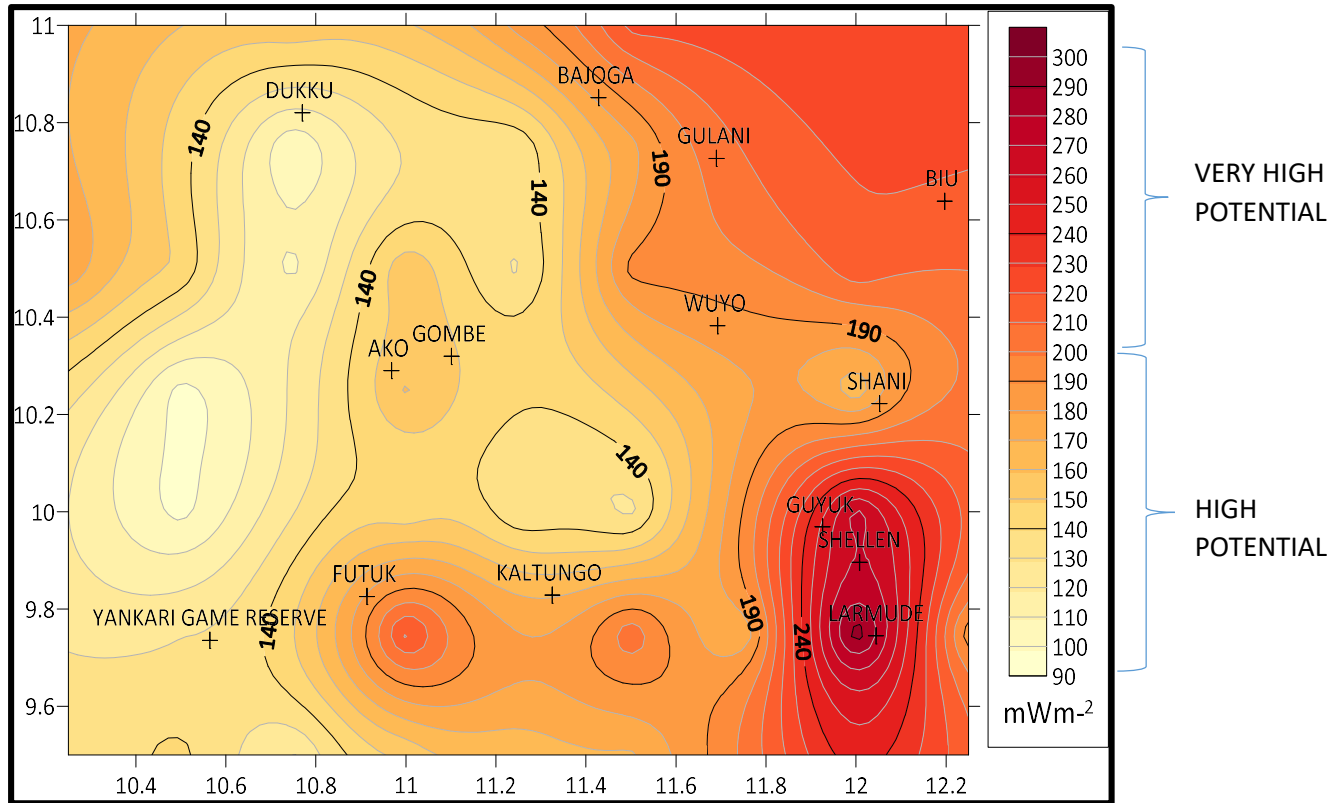


Figure 13: Heat flow distribution of the Northern Benue Trough

DISCUSSION OF RESULT

The depth to the top of the anomaly varies from 0.3km to 1.9km with an average value of 0.708163 km. The lowest depths are around Guyuk, Shellen, and Biu areas. Possibly, intrusions are imminent around the GUYUK-SHANI-SHELLEN area because of the decrease in sedimentary thickness. Depths to deeper magnetic sources (Z_0) of the study area vary from 2.7km to 8.0km with an average of 5.045km. This depth tilts greater along the Dukku-Fali-Yankari axis and less along the Gulani-Larmude axis.

The isolated CPD contour of high isocurie point depths along the Dikku - Yankari game reserve axis and low isocurie point depth around the Guyuk-Shellen-Larmude areas are spectacular. These isolated events may be attributes of the thermal history of the trough noting that the northern Benue trough has been tectonic active which possibly must have caused the variation of the crustal thickness.

The geothermal variation ranges from about 33km/ °C to 120km/ °C with an average value of 76.5km/ °C within the study area. Areas of high geothermal gradients may be suggested as having geothermal resource energy potential. Larmude-Shellen area has high geothermal energy potential whereas the area between Dukku and Yankari Game reserve is of lower geothermal energy values. From these discrepancies, the study area can be partitioned into three distinctive zones namely: low geothermal zone, intermediate geothermal zone and high geothermal zone. Lamude-Shellen area is observed as high geothermal gradient zone whereas Dikku-Yankari has the least geothermal potential. The geothermal gradient variation observed in the study was due to possible lateral changes in the lithology and respective thermal conductivity (Macgregor, 2020). It is great to note

that the observed high heat flow obviously required the existence of a heat source either from mantle plumes, or subduction and rift zones

The heat flow variation of the study area ranges from 97 mWm^{-2} to 295.91 mWm^{-2} with an average value of 194.455 mWm^{-2} . The heat source of a geothermal field is governed by a deep magmatic mass that is yet to complete its cooling path, in association with relevant young volcanism and a faulted structure. The heat flow distribution within the trough increases along the NW-SE axis and terminates with its highest values at the Larmude- Shellen areas. The Dukku-Yankari axis appears relatively cool compared with the Guyuk-Shellen-Larmude areas. In an earlier study, it was stated that the average heat flow value for the continent is about 60 mW/m^2 . Noting that high heat flow gives rise to geothermal systems therefore, areas with estimated heat flow values between 80 and 100 mW/m^2 are good geothermal resources, while values greater than 100 mW/m^2 show an indication of anomalous geothermal conditions according to Toth and Bobok (2017). The heat flow values of 90 to 300 mW/m^2 as estimated have shown that the entire study area could ascribed a geothermal zone.

CONCLUSION

Spectral depth analysis of fort-nine (49) blocks was used to evaluate aeromagnetic anomalies of the northern Benue Trough. This technique yielded two magnetic depth models. First, depth to the top of the magnetic causative body (Z_c) varies from 300 m to 1900 m for shallow anomaly sources while. The depth to the magnetic basement / deeper sources (Z_0) varies from 2700 to 8000 m . The results reveal that sediments are thinnest in the northeast parts (Biu areas) where volcanic rocks predominate but thickest in the north-western part of the study area which is possibly a sedimentary zone.

Previous studies showed that the Curie point depth is associated with the geological content of the study area (Franco and Franco, 2017). The Curie point depths and geothermal gradients of the study area have an inverse relationship such that areas with higher Curie point depths have lower geothermal gradients and areas with higher geothermal gradient match zones of lower Curie point depth. Accessing regions with Curie point depth lower than 10 km be assigned as possible geothermal zones (Eko et. al 2021). 60% area of the study, has Curie point depth shallower than 10 km as such be proscribed as a geothermal field irrespective of the nonexistence of geothermal surface manifestations. It should be noted that inadequate fluid interaction with the subsurface thermal structure at areas with high heat flow variation was responsible for the lack of surface manifestations of geothermal signatures. However, the existence of possible geothermal resources around Yankari area, a non-volcanic zone clearly indicates that the heat flow source has radiogenic origin while the high geothermal gradient covering Shellen and Larmude zones are mostly controlled by young volcanism.

Reference:

- Abdulwahab, M.; Taiwo,,A; Salako,A; Rafiu, A; Abbass, A., and Usman, A (2019) : Assessment of Geothermal Potentials In Some Parts of Upper Benue Trough Northeast Nigeria Using Aeromagnetic Data. *Journal of Geoscience, Engineering, Environment, and Technology*.
- Akinnubi,T. D and Adetona, A. A (2018). Investigation of the geothermal potential within Benue state, Central Nigeria, from radiometric and High Resolution Aeromagnetic data. *Nigerian Journal of Physics (NJP)* 27(2)
- Eko, G. E; Ismail,Y ;Noer, E; Ismail and Raj Kumar (2021): Geothermal energy assessment through the Curie point depth, geothermal gradient, and heat flow around the Akiri hot spring region in Central Nigeria. *Environmental Earth Sciences*. **1**, Article number: 115
- Franco, A and Franco, Donatini (2017). Methods for the estimation of the stored energy in geothermal resources. *Journal of Physics, series 796*.
- Ibe, Stephen Onyejiuwaka and Uche, Kelvin Iduma (2020): Assessment of Geothermal Energy Potential of Ruwan Zafi, Adamawa State and Environs, Northeastern Nigeria, using High Resolution Airborne Magnetic Data. *Current Research in Geoscience 2020, Volume 10: 1.15*
- Kasidi, S., & Nur, A. (2012). Curie depth isotherm deduced from spectral analysis of Magnetic data over Sarti and environs of North-Eastern Nigeria. *Sch J Biotech*, 1, 49-56..
- Macgregor, D.S (2020): Regional variation in geothermal and heat flow across African plate, *Journal of Earth Sciences*. Volume 171, pp19.
- Salawu,N.B; Dada,S.S; Fatoba ,J.O; Ojo,O.J; Adebisi ,L,S ; Abayomi J.S , Abdulraheem, T.Y (2021). Structural architecture of the Middle Niger Basin, Nigeria based on aeromagnetic data: An example of a non-volcanic basin. *Heliyon* Volume 7, Issue 6..
- Shehu, A. T ; Olatunji, S. and Lawal, T. O.(2016): Assessment of geothermal potential of Sokoto basin. northwestern Nigeria using spectral centroid analysis of high-resolution aeromagnetic (hram) data. *Journal of Science, Technology, Mathematics and Education (JOSTMED)*, 12(2),
- Toth, A and Bobok, E (2017): Flow and heat transfer in Geothermal system. *Science direct*. pp 363-376.

- Uche, I ; Ibe,S. O and Nwokeabia, C. N (2020). Curie depth and heat flow analysis of Ikot Ekpene and environs, Eastern Niger Delta Basin, using airborne magnetic data. *International Journal of Advanced Geosciences*, 8 (2), 263-271.
- Qudsi, Izzul (2019): Curie Point depth mapping underneath Botswana for geothermal prospect identification using aeromagnetic data . *Applied earth science*.
- Zhanxiang H.E; Liu,Y ; Suo,Xi and Dong, W (2008): Application of Magnetic Prospecting in Recognition of Volcanic Reservoirs. *Journal of Canadian Society of exploration Geophysicists*. vVolume 33, Number 01.